ETHANOL SENSORS BASED ON ZINC OXIDE SYNTHESIZED BY THE CHEMICAL PRECIPITATION METHOD

D. V. Yevdakha, A. Yu. Lyashkov*

Oles Honchar Dnipro National University, Dnipro, Ukraine
**e-mail: alexdnu@ukr.net*

We report the synthesis, structural characterization and ethanol vapor sensing performance of zinc oxide (ZnO) ceramic sensors prepared from a chemical-precipitation nanomaterial and commercial submicron ZnO powder. ZnO powder is synthesized by precipitation from zinc acetate using KOH as precipitant, dried and processed into gas-sensitive layers on a porous ceramic substrate with silver electrodes; reference sensors are prepared from industrial ZnO. Structural characterization (XRD, optical microscopy) indicates polycrystalline wurtzite ZnO; Scherrer analysis yields average crystallite sizes of ~270 nm (synthesized) and ~500 nm (commercial). Gas sensing testing is performed in a controlled measurement chamber under ethanol vapor partial pressure P_e = 37 Pa at operating temperatures from ~380 K to ~640 K. The commercial-powder sensor exhibits approximately two-times larger response across the tested temperature range, while the synthesized-powder sensor has higher baseline conductivity. The response peaks near ~ 600 K and decreases at higher temperatures. Differences are discussed in terms of grain size, chemisorbed oxygen coverage and inter-granular potential barriers affecting carrier transport. These results illustrate the complex interplay of microstructure and surface chemistry in ZnO ethanol sensing and highlight practical considerations for sensor fabrication and thermal activation.

Keywords: ZnO, ethanol sensor, metal-oxide semiconductor, response time, chemical precipitation.

Received 11.09.2025; Received in revised form 06.10.2025; Accepted 10.12.2025

1. Introduction

Metal-oxide semiconductor gas sensors based on zinc oxide (ZnO) remain among the most studied chemiresistive devices for detection of volatile organic compounds, in particular ethanol, due to their chemical stability, relatively simple fabrication and the tunability of response through morphology control and doping strategies [1]. Ethanol detection is important for breath analysis, industrial safety and environmental monitoring, and ZnO is widely used because its surface reactivity and electronic properties can be tailored by nanostructuring, noble-metal decoration or composite formation to improve sensitivity, selectivity and operating temperature [1-3].

The sensing mechanism of ZnO chemiresistors is classically attributed to oxygen chemisorption at the metal-oxide surface, which extracts electrons from the conduction band and forms an electron-depleted surface region (space-charge layer) that increases the overall resistance. Exposure to a reducing gas such as ethanol results in reaction with the adsorbed oxygen species, release of electrons back into ZnO and a consequent increase in conductance [2, 4]. The relative population of molecular (O_2^-) and atomic (O^-) adsorbed oxygen species, and thus the temperature dependence of sensing, is determined by operating temperature and surface morphology-factors that commonly set the optimal working temperature for ZnO ethanol sensors well above room temperature unless special low-temperature activation strategies (e.g., noble-metal catalysts, heterojunctions, light activation) are employed [2, 5].

Improving sensor kinetics (short response and recovery times) and lowering the operating temperature are active research directions. Approaches include reducing characteristic diffusion lengths (1D nanorods/nanofibres, thin films), forming heterojunctions or noble-metal decoration to catalyze surface reactions and accelerate charge transfer, and increasing the porosity to favor rapid gas access to the active sites [3-5]. Numerous recent experimental studies report enhanced ethanol sensitivity and faster dynamics using dopants or composites (for example ZnO-NiO, La-doped ZnO, Au/Ag decoration), demonstrating that both surface chemistry and electronic structure govern sensitivity as well as the kinetic response [2, 5-6].

Experimental details – gas concentration or partial pressure, flow rates, chamber dead-volume and valve switching times, baseline conditioning, and operating temperature – have strong influence on measured kinetics and must be reported for meaningful comparison.

In this work we investigate ethanol sensing by ceramic-type ZnO sensors fabricated from ZnO synthesized by chemical precipitation from zinc acetate, and commercial submicron ZnO powder. The goals are: to compare response magnitudes and response/recovery kinetics of sensors from the two powders, to establish the temperature dependence of sensitivity and kinetics, and to analyze observed differences in the context of grain size, baseline conductivity and surface chemisorption mechanisms. Our study complements recent work on morphological and compositional tuning of ZnO ethanol sensors and provides practical fabrication-level insight for ceramic sensor elements.

2. Synthesis of samples and experimental procedure

The ZnO-based nanomaterial was synthesized by the chemical precipitation method [7, 8]. Zinc acetate dihydrate ($C_4H_6O_4Zn \cdot 2H_2O$) was used as the precursor, and potassium hydroxide (KOH) served as the precipitating agent. Zinc acetate was dissolved in distilled water, and an aqueous KOH solution was added in the stoichiometric amount required for the complete reaction:

$$Zn(CH_3COO)_2 + 2KOH \rightarrow ZnO + 2KCH_3COO + H_2O.$$

As a result, zinc oxide (ZnO) precipitated together with potassium acetate (KCH_3COO) and water. The ZnO was deposited as a thick layer onto the substrate, which was then dried in air at room temperature. Similar precipitation routes are widely used for obtaining highly pure ZnO nanopowders with controllable particle size and surface activity [9].

During the fabrication of active sensor elements and other nanostructured devices, it is important to ensure high mechanical strength of the samples to achieve reliable electrical contact between electrodes and the nanomaterial layer, thereby providing stability of electrical parameters.

Silver electrodes were applied onto a porcelain tubular substrate (40 × 4 mm) containing two parallel channels (0,8 mm diameter) by firing a silver-paste metallization layer in air (Fig. 1). The prepared electrodes were sintered at 700 °C for 1 h [1]. The ZnO powder was mixed with an organic binder, composed of liquid paraffin and solid paraffin hydrocarbons with composition $C_{18}H_{38}$–$C_{35}H_{72}$. The space between the electrodes was filled with a ZnO-binder suspension layer about 0,5 mm thick.

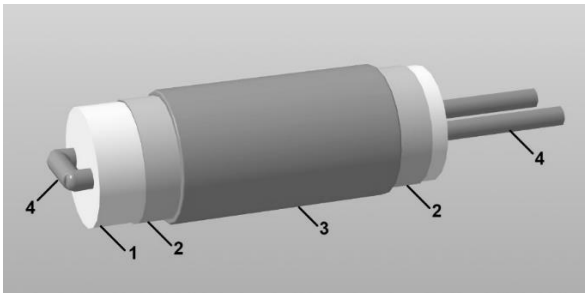

Fig. 1. Active element of the gas-sensitive sensor:
1 – porcelain substrate; 2 – silver electrodes; 3 – ZnO gas-sensitive layer; 4 – nichrome heating wire.

To remove organic constituents and enhance the mechanical strength and adhesion of the ZnO layer to the substrate, the samples were annealed at 400 °C for 1 h in air. The binder combusted completely, and the oxidation products were released as gases.

Active sensor elements were fabricated using both the chemically synthesized ZnO powder and a commercial submicron ZnO powder of analytical grade (purity “chemically pure”).

Copper-silver wires were attached to the silver electrodes and connected to the measuring circuit of the gas-sensing setup. The setup’s functional diagram is shown in Fig. 2. The test sample was placed in a sealed chamber where a required gas atmosphere was generated. Sample heating was controlled by a manually regulated laboratory autotransformer. Three digital voltmeters (V1, V2, V3, model B7-27A/1) with digital outputs were used. V1 measured the sample temperature via a chromel-copel thermocouple, while V2 and V3 measured the sensor voltage and the voltage drop across a series current resistor R, respectively. From these values, the current through the sensor was calculated using Ohm’s law.

Signals from the voltmeters were transferred via a buffer interface to a personal computer through an LPT port. A control program converted the data, displayed the conductance and temperature in real time, and stored the results for analysis.

The sensor response was defined as σ/σ_o, where σ and σ_o are the conductivities in ethanol vapor and in air, respectively. The response time (t_{resp}) was the interval required for the signal to rise from 10 % to 90 % of its maximum amplitude, and the recovery time (t_{rec}) was the interval for the signal to decay to 10 % above the baseline [5, 10].

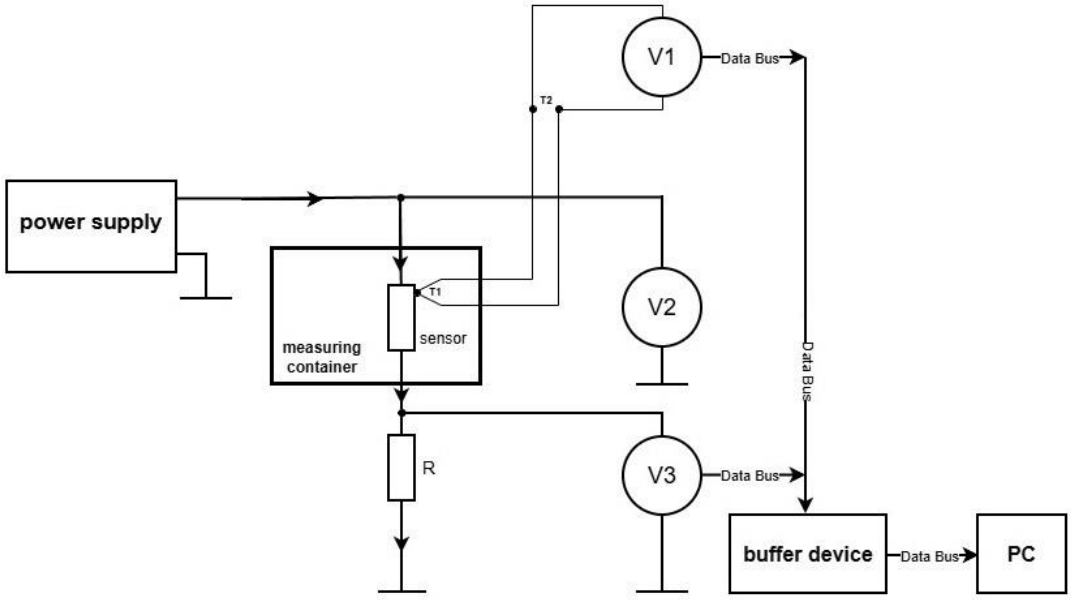

Fig. 2. Functional schematic of the experimental setup for studying gas-sensitive properties.

The desired gas atmosphere was created by introducing selected substances into the chamber in either gaseous or vapor form. For liquids, vapor was produced by controlled evaporation. The partial pressure *p* of ethanol vapor was calculated using the Clapeyron-Mendeleev equation [11]:

$$pV = \frac{m}{M}RT \quad (1)$$

where p is pressure, V is volume, m is mass, M is molar mass, R is the universal gas constant, and T is absolute temperature.

The X-ray diffraction (XRD) patterns of both synthesized and commercial ZnO powders were obtained using a DRON-2.0 diffractometer. The average crystallite size d was estimated from the broadening of diffraction peaks using the Debye-Scherrer equation [12]:

$$d = k \cdot \lambda / (\beta \cdot \cos\theta), \quad (2)$$

where d is the crystallite size, λ = 1,54178 Å (Cu Kα), β is the full width at half maximum of the peak, θ is the Bragg angle, and k = 0,9.

The microstructure of the materials was further examined using optical microscopy to assess grain morphology and homogeneity.

3. Experimental results and discussion

Optical micrographs of the ZnO powder synthesized by the chemical precipitation method before thermal treatment are shown in Figs. 3-4. The surface of the ZnO layer deposited on the substrate and dried at room temperature exhibited an irregular white morphology (Fig. 3). At the magnification of ×400, distinct inhomogeneities were observed, presumably representing individual ZnO crystallites and their agglomerates. Determination of individual crystal sizes by optical microscopy, however, was not possible due to the resolution limit.

X-ray diffraction (XRD) analysis confirmed that the synthesized material consisted solely of wurtzite-type ZnO, with no reflections corresponding to secondary phases. Calculations using Eq. (2) yielded an average crystallite size of approximately 270 nm for the synthesized material, whereas the commercial ZnO powder had an average grain size of about 500 nm, consistent with other reports on submicron ZnO ceramics [13, 14].

Fig. 3. Optical micrograph of the ZnO layer obtained by chemical precipitation (×100).

Fig. 5 show the kinetics of the sensor response (σ/σ_0) fabricated from the chemically precipitated powder. Upon introduction of the sample into air containing ethanol vapor (C_2H_5OH), its electrical conductivity increased rapidly and then approached a quasi-steady value. However, for certain sensor temperatures (450–600 K), conductivity continued to vary throughout the 300 s measurement period. Therefore, the response magnitude was evaluated 300 s after exposure began. The partial pressure of ethanol vapor (P_e) in the chamber was maintained at 37 Pa.

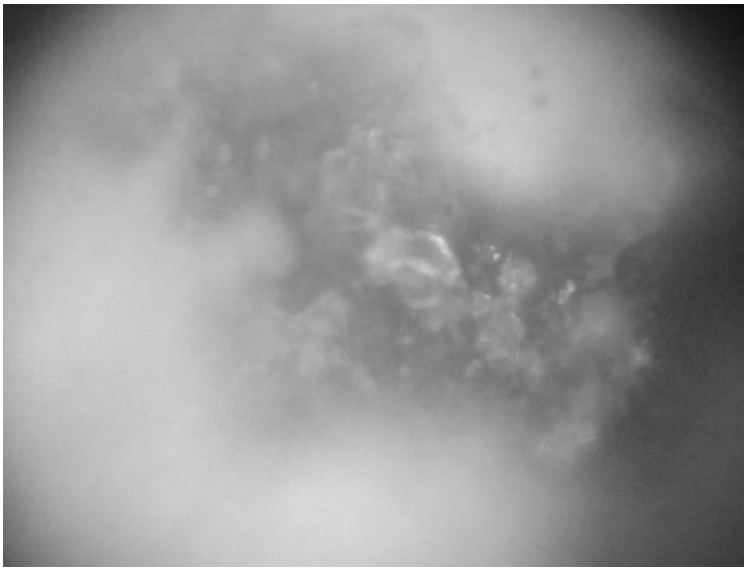

Fig. 4. Optical micrograph of the ZnO layer obtained by chemical precipitation (×400).

When the sensor was removed from the ethanol atmosphere, the conductivity decreased and nearly returned to its initial baseline value (σ_o). The sensor response increased moderately with temperature. From the kinetic curves, both the response and recovery times were determined (Table 1). For the sensor fabricated from the commercial ZnO powder, the overall response kinetics followed the same trends as those of the sensor prepared from the synthesized powder (Table 1).

Table 1

Gas-sensing parameters of ZnO sensors in ethanol vapor (P_e = 37 Pa)

Material	*T*, K	σ/σ_o	t_{resp}, s	t_{rec}, s
Synthesized	386	2,67	71	125
Synthesized	455	2,83	96	88
Synthesized	512	3,6	98	79
Synthesized	595	6,05	>300	101
Synthesized	643	4,16	49	111
Commercial	384	6,77	68	62
Commercial	455	12	131	120
Commercial	516	13,4	95	72
Commercial	600	14	>300	112
Commercial	640	12,75	96	91

Based on Table 1, the temperature dependence of sensor response was plotted (Fig. 6). As can be seen, the response of the sensor fabricated from commercial ZnO powder was approximately twice that of the sensor based on the synthesized material over the entire temperature range.

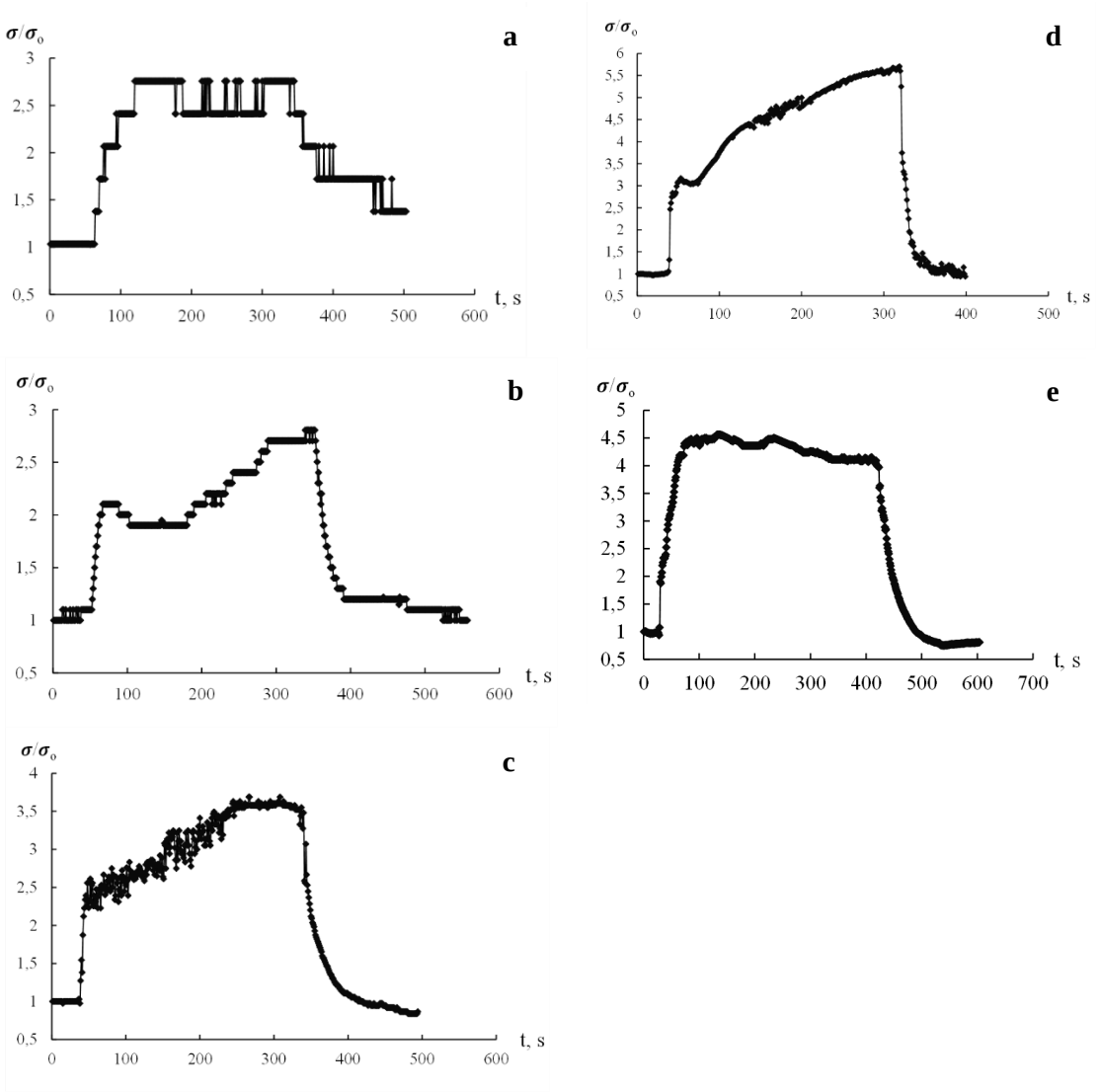

Fig. 5. Typical temporal dependences of ZnO sensor conductance in ethanol vapor at various sensor temperatures: a – 386 K; b – 455 K; c – 512 K; d – 595 K; e – 643 K (P_e = 37 Pa).

As evident from Fig. 6, the response increased with rising temperature, reaching a maximum near 600 K, followed by a decline at higher temperatures.

According to numerous studies [15-17], oxygen is chemisorbed on the ZnO surface in charged molecular (O_2^-) and atomic (O^-) forms. The ratio between these species depends strongly on temperature. At lower temperatures, molecular O_2^- species dominate, whereas at higher temperatures atomic oxygen ions prevail. Oxygen chemisorption leads to the formation of an electron-depleted surface layer around ZnO crystallites, resulting in inter-grain potential barriers and a decrease in overall conductivity of the ceramic [10, 18].

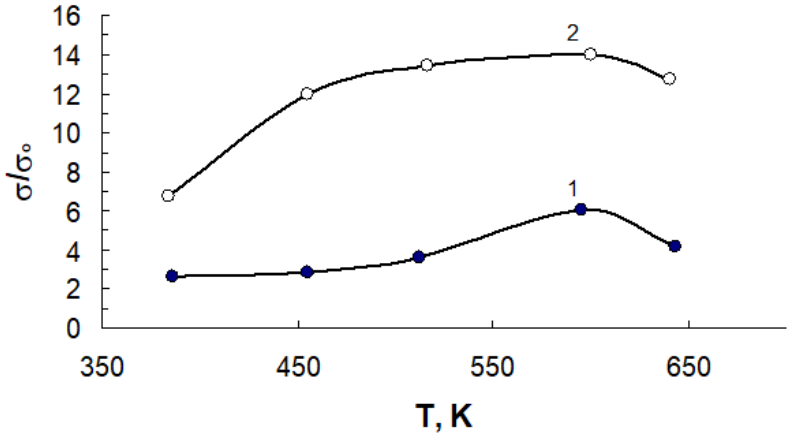

Fig. 6. Temperature dependence of response magnitude for ZnO sensors: 1 – synthesized ZnO; 2 – commercial ZnO (P_e = 37 Pa, measurement time = 300 s).

When the sensor is exposed to an ethanol-containing atmosphere, ethanol molecules are adsorbed on the ZnO surface and can react with the chemisorbed oxygen species according to the well-established reaction mechanism [11]:

$$C_2H_5OH + 3O^- \rightarrow 2CO_2 + 3H_2O + 3e^-. \quad (3)$$

Electrons released in reaction (3) return to the conduction band of ZnO, increasing the conductivity of the sensor. After removal of ethanol vapor, the chemisorbed oxygen layer is restored, and the conductivity decreases again. This mechanism explains the reversible behavior of ZnO-based ethanol sensors [11].

The response of the sensor based on commercial ZnO was roughly twice that of the synthesized-powder sensor throughout the temperature range. Nevertheless, XRD and microscopy showed that the synthesized ZnO possessed smaller grains (~ 270 nm) compared with the commercial powder (~ 500 nm), which theoretically should provide a larger specific surface area and thus higher sensitivity.

The measured electrical conductivity of the sensor from commercial powder was 4.79×10^{-9} Ohm^{-1}, while that of the synthesized nanopowder sample was 2.87×10^{-8} Ohm^{-1}. Given identical geometry, conductivity reflects the intrinsic material properties. The higher response of the commercial ZnO can therefore be attributed to stronger inter-crystallite potential barriers and a greater density of chemisorbed oxygen species compared with the synthesized ZnO. A smaller amount of chemisorbed oxygen on the surface of the chemically precipitated ZnO grains likely leads to a weaker modulation of conduction upon exposure to ethanol, resulting in a smaller response amplitude.

4. Conclusions

Zinc oxide–based ceramic sensors prepared from both chemically precipitated and commercial powders were investigated for ethanol vapor detection. The synthesized ZnO demonstrated smaller crystallite size (~ 270 nm) compared with commercial ZnO (~ 500 nm), yet the sensor fabricated from the commercial powder exhibited nearly double the response

magnitude across the 386–643 K range. Both sensor types displayed similar kinetic behaviour: the response increased with temperature, reaching a maximum around 600 K, followed by a decline at higher temperatures.

The observed differences are interpreted in terms of grain-boundary potential barriers and surface chemisorption of oxygen. Higher baseline conductivity of the synthesized material suggests reduced oxygen coverage and weaker barrier formation, resulting in lower sensitivity. In contrast, the commercial ZnO exhibits stronger chemisorption and larger barriers, enhancing modulation of conductance upon ethanol exposure.

These findings confirm that not only grain size but also surface state and microstructural integrity critically determine the response of ZnO-based ethanol sensors. The results support the optimization of synthesis and post-treatment conditions to control oxygen vacancies and grain connectivity, which can lead to improved sensitivity and faster response at moderate operating temperatures.

References

1. **Dey, A.** Semiconductor metal oxide gas sensors: A review / A. Dey // Materials Science in Semiconductor Processing. – 2018. – Vol. 229. – P. 206 – 217. DOI: 10.1016/j.mseb.2017.12.036

2. **Wang, P.** Recent advances in resistive gas sensors / P. Wang, S. Xu, X. Shi, J. Zhu, H. Xiong, H. Wen // Sensors. – 2025. – Vol. 13(7). – P. 224. DOI: 10.3390/chemosensors13070224

3. **Dutta, T.** Road map of semiconductor metal-oxide-based sensors / T. Dutta, T. Noushin, S. Tabassum, S. K. Mishra // Sensors. – 2023. – Vol. 23(15). – P. 6849. DOI: 10.3390/s23156849

4. **Goel, N.** Metal oxide semiconductors for gas sensing / N. Goel, K. Kunal, A. Kushwaha, M. Kumar // Engineering Reports. – 2023. – P. 1 – 10. DOI: 10.1002/eng2.12604

5. **Ponzoni, A.** A statistical analysis of response and recovery times in gas sensors / A. Ponzoni // Sensors. – 2022. – Vol. 22(17). – P. 6346. DOI: 10.3390/s22176346

6. **Suzuki, T. T.** Ethanol gas sensing by a Zn-terminated ZnO (0001) bulk surface: a theoretical study / T. T. Suzuki, T. Ohgaki, Y. Adachi, I. Sakaguchi, M. Nakamura, H. Ohashi, A. Aimi, K. Fujimoto // ACS Omega. – 2020. – Vol. 5. – P. 21104 – 21112. DOI: 10.1021/acsomega.0c02750

7. **Lee, K. S.** Electrochemical properties and characterization of various ZnO structures using a precipitation method / K. S. Lee, C. W. Park, J. D. Kim // Colloids and Surfaces A: Physicochemical and Engineering Aspects. – 2017. – Vol. 512. – P. 87 – 92. DOI: 10.1016/j.colsurfa.2016.10.022

8. **Aalami, Z.** Synthesis, characterization, and photocatalytic activities of green sol-gel ZnO nanoparticles using Abelmoschus esculentus and Salvia officinalis: A comparative study versus co-precipitation-synthesized nanoparticles / Z. Aalami, M. Hoseinzadeh, P. Hosseini Manesh, A.H. Aalami, Z. Es'haghi, M. Darroudi, A. Sahebkar, H.A. Hosseini // Heliyon. – 2024. – Vol. 10(2). – P. e24212. DOI: 10.1016/j.heliyon.2024.e24212

9. **Caballero, A. C.** Controlled precipitation methods: formation mechanism of ZnO nanoparticles / A. C. Caballero, M. Villegas, C. Moure, J. F. Fernández // Journal of the European Ceramic Society. – 2001. – Vol. 21. – P. 925 – 930. DOI: 10.1016/S0955-2219(00)00283-1

10. **Tonkoshkur, A. S.** Kinetics of response of ZnO–Ag ceramics for resistive gas sensor to methane, and its analysis using a stretched exponential function / A. S. Tonkoshkur, A. Yu. Lyashkov, E. L. Povzlo // Sensors and Actuators B: Chemical. – 2018. – Vol. 255. – P. 1680 – 1686. DOI: 10.1016/j.snb.2017.08.17111.

11. **Lyashkov, A. Yu.** Gas sensitivity of ZnO-based ceramics to vapors of saturated monohydric alcohols / A. Yu. Lyashkov, A. S. Tonkoshkur // Materials Chemistry and Physics. – 2013. – Vol. 140(1). – P. 31 – 36. DOI: 10.18668/NG.2023.02.02

12. **Cullity, B. D.** Elements of X-ray diffraction / B. D. Cullity, S. R. Stock – 3rd ed. – New Jersey: Prentice Hall, 2001.

13. **Xu, J.** Grain size control and gas sensing properties of ZnO gas sensor / J. Xu, Q. Pan, Y. Shun, Z. Tian // Sensors and Actuators B: Chemical. – 2000. – Vol. 66. – P. 277 – 279. DOI: 10.1016/S0925-4005(00)00381-6

14. **Phan, D. T.** Effects of different morphologies of ZnO films on hydrogen sensing properties / D. T. Phan, G. S. Chung // Journal of Electroceramics. – 2014. – Vol. 32. – P. 353 – 360. DOI: 10.1007/s10832-014-9911-7

15. **Wang, J.** Synergistic effects of UV activation and surface oxygen vacancies on NO_2 sensing / J. Wang, Y. Shen, X. Li, Y. Xia, C. Yang // Sensors and Actuators B: Chemical. – 2019. – Vol. 298. – P. 126858. DOI: 10.1016/j.snb.2019.126858

16. **Brahma, S.** Optical response of ZnO nanorods induced by oxygen chemisorption and desorption / S. Brahma, C. W. Yang, C. H. Wu, F. M. Chang, T. J. Wu, C. S. Huang, K. Y. Lo // Sensors and Actuators B: Chemical. – 2018. – Vol. 259. – P. 900 – 907. DOI: 10.1016/j.snb.2017.12.093

17. **Gotra, Z. Yu.** Microelectronic sensors of physical quantities / Z. Yu. Gotra (Ed.) – Lviv: Liga-Press, 2003. – Vol. 2.– 595 p.

18. **Kovalenko, O. V.** Features of gas environment influence on electrical properties of ZnO / O. V. Kovalenko, V. Yu. Vorovsky, A. Yu. Lyashkov // Journal of Physics and Electronics. – 2023. – Vol. 31(2). – P. 57 – 62. DOI: 10.15421/332320